Electronic Conductivity of Solid-State, Mixed-Valent, Monolayer-Protected Au Clusters

W. Peter Wuelfing, Stephen J. Green,† Jeremy J. Pietron,‡ David E. Cliffel,§ and Royce W. Murray*

Contribution from the Kenan Laboratories of Chemistry, University of North Carolina, Chapel Hill, North Carolina 27599-3290

Abstract: Electronic conductivity, σ_{EL}, in solid-state films of alkanethiolate monolayer protected Au clusters (Au MPCs) occurs by a bimolecular, electron self-exchange reaction, whose rate constant is controlled by (a) the core-to-core tunneling of electronic charge along alkanethiolate chains and (b) the mixed valency of the MPC cores (e.g., a mixture of cores with different electronic charges). The tunneling mechanism is demonstrated by an exponential relation between the electronic conductivity of $Au_{309}(C_n)_{92}$ MPCs (average composition) and n, the alkanethiolate chainlength, which varies from 4 to 16. The electron tunneling coefficient $\beta_n = 1.2/CH_2$ or, after accounting for alkanethiolate chain interdigitation, $\beta_{dis} = 0.8$ Å^{-1}. Quantized electrochemical double layer charging of low polydispersity $Au_{140}(C6)_{53}$ MPCs was used to prepare solutions containing well-defined mixtures of MPC core electronic charges (such as MPC^0 mixed with MPC^{1+}). Electronic conductivities of mixed-valent, solid-state $Au_{140}(C6)_{53}$ MPC films cast from such solutions are proportional to the concentration product [MPC^0][MPC^{1+}], and give a MPC$^{0/1+}$ electron self-exchange rate constant of ca. 10^{10} M^{-1} s^{-1}.

Introduction

The properties of nanometer-sized particles are of intense contemporary interest, driven by both fundamental questions and possibilities for use in nanoscale technology. A significant literature base[1] has emerged on semiconductor nanoparticles (such as CdS); nanoparticles based on metallic elements (e.g., Au, Ag, Pd, etc.) comprise a lesser but growing literature.[2] Reported properties include transitions between insulator and conductor[3] and metallic and molecular behaviors,[4] assembly of molecular tunneling bridges to nanoparticles,[5] and single-electron charging,[4a,6] to name a few.

A substantial impetus is given to nanoparticle investigations by synthetic strategies that yield well-defined, stable materials. A nanoparticle synthesis reported by Schiffrin and co-workers[7] involved passivating 1−5 nm Au clusters with a dense, robust monolayer of alkanethiolates. We call[2a] these materials "monolayer protected clusters" (MPCs), in emphasis of their resistance to metal aggregation even in solvent-free forms. MPCs are like large molecular entities and can be subjected to poly-derivatization reactions.[2c] These attributes have enabled a variety of investigations of their electronic,[2h,j,8] optical,[9] and electro-

† Present address: School of Chemistry, Stocker Road, University of Exeter, Exeter EX4 4QD, UK.

‡ Present address: Naval Research Laboratory, 4555 Overlook Ave. S.W., Washington, DC 20375.

§ Present address: Vanderbilt University, 201 West End Avenue, Nashville, TN 37235.

(1) (a) Gorer, S.; Penner, R. M. *J. Phys. Chem. B* **1999,** *103,* 5750−5753. (b) Burda, C.; Green, T. C.; Link, S.; El-Sayed, M. A. *J. Phys. Chem. B* **1999,** *103,* 1783. (c) Klein, D. L.; Roth, R.; Lim, A. K. L.; Alivisatos, A. P.; McEuen, P. L. *Nature* **1997,** *389,* 699. (d) Mews, A.; Banin, U.; Kadavanich, A. V.; Alivasatos, A. P. *Ber. Bunsen-Ges. Phys. Chem., Int. J. Phys. Chem.* **1997,** *101,* 1621.

(2) (a) Templeton, A. C.; Wuelfing, W. P.; Murray, R. W. *Acc. Chem. Res.* **2000,** *1,* 27. (b) Whetten, R. L.; Shafigulin, M. N.; Khoury, J. T.; Schaff, T. G.; Vezmar, I.; Alvarez, M. M.; Wilkinson, A. *Acc. Chem. Res.* **1999,** *32,* 397. (c) Templeton, A. C.; Hostetler, M. J.; Warmoth, E. K.; Chen, S.; Hartshorn, C. M.; Krishnamurthy, V. M.; Forbes, M. D. E.; Murray, R. W. *J. Am. Chem. Soc.* **1998,** *120,* 4845−4849. (d) Templeton, A. C.; Hostetler, M. J.; Kraft, C. T.; Murray, R. W. *J. Am. Chem. Soc.* **1998,** *120,* 1906−1911. (e) Schaaff, T. G.; Shafigullin, M. N.; Khoury, J. T.; Vezmar, I.; Whetten, R. L.; Cullen, W.; First, P. N.; Gutierrez-Wing, C.; Ascensio, J.; Jose-Yacaman, M. J. *J. Phys. Chem. B* **1997,** *101,* 7885−7891. (f) Wuelfing, W. P.; Templeton, A. C.; Hicks, J. F.; Murray, R. W. *Anal. Chem.* **1999,** *71,* 4069−4074. (g) Baum, T.; Bethell, D.; Brust, M.; Schiffrin, D. J. *Langmuir* **1999,** *15,* 866. (h) Gittens, D. I.; Bethell, D.; Nichols, R. J.; Schiffrin, D. J *J. Mater. Chem.* **1999,** *0,* 1. (i) Luedtke, W. D.; Landman, U. *J. Phys. Chem. B* **1998,** *102,* 6566. (j) Brust, M.; Bethell, D.; Kiely, C. J.; Schiffrin, D. J. *Langmuir* **1998,** *14,* 5425−5429. (k) Schon, G.; Simon, U. *Colloid Polym. Sci.* **1995,** *2,* 101. (l) Schon, G.; Simon U. *Colloid Polym. Sci.* **1995,** *273* (3), 202. (m) Zamborini, F. P.; Hicks J. F.; Murray, R. W. *J. Am. Chem. Soc.* **2000,** *122,* 4514. (n) Chen, S. W.; Murray, R. W. *J. Phys. Chem.* **1999,** *103,* 9996. (o) Templeton, A. C.; Cliffel, D. E.; Murray, R. W. *J. Am. Chem. Soc.* **1999,** *121,* 7081. (p) Green, S. J.; Stokes, J. J.; Hostetler, M. J.; Pietron, J. J.; Murray, R. W. *J. Phys. Chem. B* **1997,** *101,* 2663.

(3) (a) Collier, C. P.; Saykally, R. J.; Shaing, J. J.; Henrichs, S. E.; Heath, J. R. *Science* **1997,** *277,* 1978. (b) Markovich, G.; Collier, C. P.; Heath, J. R. *Phys. Rev. Lett.* **1998,** *17,* 3807.

(4) (a) Chen, S.; Ingram, R. S.; Hostetler, M. J.; Pietron, J. J.; Murray, R. W.; Schaaff, T. G.; Khoury, J. T.; Alvarez, M. M.; Whetten, R. L. *Science* **1998,** *280,* 2098. (b) Alvarez, M. M.; Khoury, J. T.; Schaaff, T. G.; Shafigullin, M. N.; Vezmar, I.; Whetten, R. L. *J. Phys. Chem. B* **1997,** *19,* 3706. (c) Schaff, T. G.; Schafigullin, M. N.; Khoury, J. T.; Vezmar, I.; Whetten, R. L.; Cullen, W. G.; First, P. N.; Gutierez-Wing, C.; Ascensio, J.; Jose-Yacaman, M. J. *J. Phys. Chem. B* **1997,** *101,* 7885.

(5) Chung, S.-W.; Markovich, G.; Heath, J. R. *J. Phys. Chem. B* **1998,** *35,* 6687.

(6) (a) Hicks, J. F.; Templeton, A. C.; Chen, S.; Sheran, K. M.; Jasti, R.; Murray, R. W. *Anal. Chem.* **1999,** *71,* 3703. (b) Chen, S.; Murray, R. W.; Feldberg, S. W. *J. Phys. Chem. B* **1998,** *102,* 9898. (c) Ingram, R. S.; Hostetler, M. J.; Murray, R. W.; Schaff, T. G.; Khoury, J. T.; Whetten, R. L.; Bigioni, T. P.; Guthrie, D. K.; First, P. N. *J. Am. Chem. Soc.* **1997,** *119,* 9279. (d) Feldheim, D. L.; Keating, C. D. *Chem. Soc. Rev.* **1998,** *27,* 1. (e) Sato, T.; Ahmed, H.; Brown, D.; Johnson, B. F. G. *J. Appl. Phys.* **1997,** *696.* (f) Feldheim, D. L.; Grabar, K. C.; Natan, M. J.; Mallouk, T. E. *J. Am. Chem. Soc.* **1996,** *118,* 7640.

(7) Brust, M.; Walker, M.; Bethel, D.; Schiffrin, D. J.; Whyman, R. *J. Chem. Commun.* **1994,** 801−802.

(8) Terrill, R. H.; Postlethwaite, T. A.; Chen, C.-C.; Poon, C.-D.; Terzis, A.; Chen, A.; Hutchison, J. E.; Clark, M. R.; Wignall, G.; Londono, J. D.; Superfine, R.; Falvo, M.; Johnson, C. S.; Samulski, E. T.; Murray, R. W. *J. Am. Chem. Soc.* **1995,** *117,* 12537.

(9) Templeton, A. C.; Pietron, J. J.; Mulvaney, P.; Murray, R. W. *J. Phys. Chem B* **2000,** *104,* 564.

chemical[2m,n,o,p,4a,6a,b,c] properties. This paper focuses on the electronic conductivity of solid-state MPCs, in particular on effects (a) of the initial charge state of the Au cores of the MPC sample and (b) of the alkanethiolate monolayer chain length.

While the effect of mixed valency on the electronic conductivity of dry (solid state) redox polymers is well-established,[10] that for MPCs has not been described. There are likewise few reports on other kinds of core-charge effects; excess charge has been shown[1c] to influence properties of quantum dots in single electron charging experiments. It has been amply demonstrated that electron transport in solid-state, mixed-valent redox polymers[10,11] occurs by bimolecular electron self-exchange (e.g., "hopping"). We propose that this kinetic picture is also appropriate to describe the electronic conductivity of "mixed-valent" MPCs.

The mixed-valent hypothesis is explored by preparing solid-state films of MPCs of average composition $Au_{140}(C6)_{53}$ that contain various mixtures of different core electronic charge states (e.g., $MPC^{2+/1+}$, $MPC^{1+/0}$, $MPC^{0/1-}$). "Mixed valent" is used simply to refer to charge state mixtures—these materials could alternatively be discussed as being doped with electron or hole charge carriers. By analogy to redox polymer conductivity, MPC electronic conductivity is cast as an electron self-exchange reaction, i.e.,

$$MPC^0 + MPC^{1+} \xrightarrow{k_{ex}} MPC^{1+} + MPC^0 \qquad (1)$$

where k_{EX} is the bimolecular rate constant ($M^{-1} s^{-1}$). The rate of reaction 1, i.e., the conductivity, should be proportional to the concentration product $[MPC^0][MPC^+]$, and be maximized when the concentrations of the two reactants are equal (i.e., 1:1 mixed valency).

Quantized electrochemical double layer charging[4a,6a,b,c] is the basis for the essential step of defining the charge states of MPCs in the solid-state $Au_{140}(C6)_{53}$ sample. This material is not perfectly monodisperse, but has a substantial population of 1.6 nm diameter, $Au_{140}(C6)_{53}$, cores. In CH_2Cl_2/electrolyte solutions, the small core dimension and low monolayer dielectric constant of this MPC combine to yield a sub-aF MPC capacitance, which in turn leads to voltammetrically[6a,b,c,2m] well-defined one-electron core charging steps and pseudo-formal potentials, $E^{o\prime}$, of core charge state "couples". The $E^{o\prime}$ values are spaced by ca. 300 mV. Using the Nernst equation, the rest potential of a solution of core-charged MPCs can be used to calculate its composition in terms of MPC core charge states. Solid-state, mixed-valent MPC films are cast from these solutions onto interdigitated array electrodes (IDAs) for conductivity measurements. The actual charging of the MPC CH_2Cl_2 solutions is done by liquid–liquid interfacial electron transfers with an aqueous cerium(IV) sulfate solution.

Reaction 1 is anticipated[12,13] to occur by electron tunneling between adjacent Au MPC cores, the monolayer serving as the tunneling barrier. There are ample experimental analogies to this process, including tunneling between an electrode and a

monolayer of a redox moiety attached to it by an alkanethiolate chain.[14] We[8] and Schiffrin et al.[2j] have reported that MPC conductivities change exponentially with chain length, behavior supporting a tunneling conductivity mechanism. The data in those reports were sparse, however, each drawing on only three differing alkanethiolate chain lengths. This report expands the previous analysis of chain length effects with measurements on MPCs with eight different alkanethiolate monolayer chain lengths of average composition $Au_{309}(C_n)_{92}$, where $n = 4, 5, 6, 7, 8, 10, 12,$ and 16. These MPCs have polydisperse core diameters (ca. 2.2 nm average) and do not exhibit observably quantized core-charging, so measured conductivities are of MPCs with ostensibly uncharged, or undoped, cores. The electron tunneling constant obtained ($\beta_{dis} = 0.8$ Å^{-1}) after taking account of chain interdigitation[2i,15] is consistent with previous[13,14] values for saturated chains.

Thermal activation results for the $Au_{309}(C_n)_{92}$ MPC conductivities are compared to predictions of Marcus[13] and granular metal[12] theories.

Experimental Section

Synthesis. MPCs were made as described previously.[15a] Briefly, $HAuCl_4$ is phase-transferred into toluene with a quaternary alkylammonium phase transfer agent, the alkanethiol is added, forming a $(Au^I$-$SC_n)_x$ polymer,[16] followed by addition of BH_4^- (again phase-transferred), which produces MPCs by a process thought[2a,17] to be a core nucleation-growth-passivation sequence. MPCs for the mixed-valent conductivity experiments were prepared using a 3:1 thiol:$AuCl_4^-$ reactant mole ratio, and have[15a] 1.6 ± 0.4 nm core diameters (by transmission electron microscopy) and an average formula of Au_{140}-$(C6)_{53}$ (assuming a truncated octahedral core geometry[2a,b,15a]). MPCs for the chain length studies were prepared using a 1:1 thiol:$AuCl_4^-$ reactant mole ratio, and have 2.2 ± 0.7 nm average core diameters and an average formula[8,15a] of $Au_{309}(C_n)_{92}$ (where $n = 4, 5, 6, 7, 8, 10, 12,$ and 16).

The as-prepared $Au_{140}(C6)_{53}$ MPCs in this study are already negatively charged; rest potentials of their solutions are negative relative to the ca. -0.2 V potential of zero charge (PZC). Presumably this is a residual effect of the reducing agent used in the synthesis. Rest potentials of the $Au_{309}(C_n)_{92}$ solutions were not measured; these data were collected before those for $Au_{140}(C6)_{53}$ MPCs and before the possible significance of rest potentials was recognized.

Chemicals. All chemicals were reagent grade and used as received.

Electrochemistry. Differential pulse voltammetry (DPV) and rest potentials of MPC solutions were measured with a BAS-100B/W electrochemical analyzer. The single compartment cell contained a 0.6

(10) (a) Sosnoff, C. S.; Sullivan, M.; Murray, R. W. *J. Phys. Chem.* **1994**, *98*, 13643. (b) Terrill, R. H.; Hutchinson, J. E.; Murray, R. W. *J. Phys. Chem. B* **1997**, *101*, 1535. (c) Any hypothetical lattice model will be inadequate to exactly account for the polydispersity of the Au_{309} cores or how they pack in a solid-state sample. This, and the lack of response of conductivity to melting (Figure 4) for the C12 and C16 MPCs, makes it inappropriate to choose between sophisticated packing structures such as hcp, or fcc, that are core size dependent.[2b] We have thus employed the simpler cubic lattice model used before.

(11) (a) Ritchie, J. E.; Murray, R. W. *J. Am. Chem. Soc.* **2000**, *122*, 2964. (b) Dickinson, E.; Masui, H.; Williams, M. E.; Murray, R. W. *J. Phys. Chem. B* **1999**, *103*, 11028. (c) Masui, H.; Long, J. W.; Malik, J.; Murray, R. W. *J. Am. Chem. Soc.* **1997**, *119*, 1997.

(12) (a) Abeles, B.; Sheng, P.; Coutts, M. D.; Arie, Y. *Adv. Phys.* **1975**, *24*, 407. (b) Sheng, P.; Abeles, B.; Arie, Y. *Phys. Rev. Lett.* **1973**, *1*, 44. (c) Sheng, P.; Abeles, B. *Phys. Rev. Lett.* **1972**, *1*, 34. (d) Neugebauer, C. A.; Webb, M. B. *J. Appl. Phys.* **1962**, *1*, 74. (e) Miller, N. C.; Hardiman, B.; Shirn, G. A. *J. Appl. Phys.* **1970**, *4*, 1850. (f) Neugebauer, C. A. *Thin Solid Films* **1970**, *6*, 443. (g) Cohen, M. H.; Douglas, M.; Currin, N.; Jortner, J. *Phys. Rev. Lett.* **1973**, *15*, 699. (h) Gittleman, J. I.; Goldstein, Y.; Bozowski, S. *Phys. Rev. B* **1972**, *9*, 3609. (i) Zeller, H. R. *Phys. Rev. Lett.* **1972**, *22*, 1452.

(13) (a) Marcus, R. A. *Angew. Chem., Int. Ed. Engl.* **1993**, *32*, 1111. (b) Marcus, R. A.; Sutin, N. *Biochim. Biophys. Acta* **1985**, *811*, 265. (c) Newton, M. D. *Chem. Rev.* **1991**, *91*, 767.

(14) (a) Smalley, J. F.; Feldberg, S. W.; Chidsey, C. E. D.; Linford, M. R.; Newton, M. D.; Liu, Y.-P. *J. Am. Chem. Soc.* **1995**, *117*, 1. (b) Sachs, S. B.; Dudek, S. P.; Hsung, R. P.; Sita, L. R.; Smalley, J. F.; Newton, M. D.; Feldberg, S. W.; Chidsey, C. E. D. *J. Am. Chem. Soc.* **1997**, *119*, 10563–10564. (c) Chidsey, C. E. D. *Science* **1991**, *251*, 920.

(15) (a) Hostetler, M. J.; Wingate, J. E.; Zhong, C.-J.; Harris, J. E.; Vachet, R. W.; Clark, M. R.; Londono, J. D.; Green, S. J.; Stokes, J. J.; Wignall, G. D.; Glish, G. L.; Porter, M. D.; Evans, N. D.; Murray, R. W. *Langmuir* **1998**, *14*, 17. (b) Badia, A.; Cuccia, L.; Demers, L.; Morin, F.; Lennox, R. B. *J. Am. Chem. Soc.* **1997**, *119*, 2682.

(16) Wuelfing, W. P.; Krisnamurthy, V.; Fisher, M.; Hostetler, M. J.; Murray, R. W. Manuscript in preparation.

(17) Chen, S. W.; Templeton, A. C.; Murray, R. W. *Langmuir* **2000**, *16*, 3543.

mm diameter Pt working electrode, a Pt coil counter electrode, and a Ag/Ag$^+$(0.01 M in CH$_3$CN) reference electrode. The potential of the Ag/Ag$^+$ reference electrode is ca. −50 mV relative to the Ag/AgCl wire quasireference electrode used previously.[18,6a,b]

Interdigitated Array Electrodes. Solid-state conductivity measurements were made using IDAs (see illustrative schematic in Figure S-1) from Microsensor Systems, Inc. (50 Au fingers, 15 μm finger width, 15 μm gap between fingers, 4800 μm finger length, 0.1 μm finger height) and Nippon Telephone and Telegraph (NTT) (100 Au fingers, 3 μm finger width, 5 μm gap between fingers, 2000 μm finger length, 0.1 μm finger height). In calculating conductivities, the IDAs are treated as parallel plate electrodes, with total areas of electrode fingers facing one another across the IDA gap[19]

$$A_{TOTAL} = A_{FINGER}(N - 1) \tag{2}$$

where N equals the number of IDA fingers. The geometric cell constant [gap distance (cm)/area$_{Total}$ (cm^2)] is 6.25 cm^{-1} for the Microsystems Inc. IDAs and 1.25 cm^{-1} for NTT IDAs.

Preparation of Mixed-Valent Au$_{140}$(C6)$_{53}$ MPC Solutions. Ten milliliters of an aqueous solution 5 mM in Ce(SO$_4$)$_2$ and 0.1 M in NaClO$_4$ was, for a selected time period, stirred rapidly, forming an emulsion in a scintillation vial with 6 mL of a CH$_2$Cl$_2$ solution 0.1 mM in Au$_{140}$(C6)$_{53}$ MPC and 0.05 M in Bu$_4$N$^+$ClO$_4^-$ electrolyte. The phases were separated, and the rest potential of the mixed-valent CH$_2$-Cl$_2$ solution of MPCs was measured in a scintillation vial at a clean Pt electrode vs Ag/Ag$^+$ reference electrode.[18] More positive rest potentials (more positive MPC core charges) result from longer contact times with the Ce(SO$_4$)$_2$ solution. The CH$_2$Cl$_2$ solvent was removed by rotary evaporation, and the Bu$_4$N$^+$ClO$_4^-$ electrolyte was extracted from the mixed-valent MPC sample with five 20 mL portions of acetonitrile, in which alkanethiolate MPCs are not soluble (shaking by hand, allowing MPC particles to settle for 5 min, and decanting). Removal of the Bu$_4$N$^+$ClO$_4^-$ electrolyte was confirmed by NMR.[20] Perchlorate is presumed to be the counterion of the positively charged MPCs. The most positively charged MPCs (those with solution rest potentials 223 and 115 mV vs Ag/Ag$^+$) are solubilized[21] by acetonitrile, so the Bu$_4$N$^+$ClO$_4^-$ electrolyte was omitted from the procedure in those cases. The details of reactions that electronically charge MPC cores are still under study.

Electronic Conductivities. Mixed-valent MPC films were cast onto a clean IDA electrode (Figure S-1), using three droplets of a concentrated MPC solution in toluene (20 mg/0.1 mL) and drying after each. The film thicknesses (ca. 15 μm, by stylus profilometry, Tencor Alpha-Step 100) are much greater than the IDA finger height. Conductivities measured for films cast with just two droplets were identical to those prepared using three. The coated IDAs are mounted on a temperature stage in a vacuum chamber and held at 30 °C for approximately 10 min to ensure dryness. The temperature was then lowered to an initial value, typically between −50 and −100 °C, and then raised in 10 °C increments, equilibrating for 20 min at each temperature before measuring the conductivity. Conductivities of well-dried MPC films were measured as previously,[8] using linear potential sweeps, which produce current−potential responses such as that shown in Figure 1. Conductivities (σ_{EL}) were measured from the slope, $\Delta i/\Delta E$ (Ω^{1-}), in the linear portion of the curve, between zero and ca. ±200 mV, and were calculated from

$$\sigma_{EL} = \frac{d\Delta i}{A_{TOTAL}\Delta E} \tag{3}$$

where d = IDA gap (cm). Voltage scans were initiated at 0 V bias and

Figure 1. Typical current−potential curve, at 30 °C, for a MPC film on an IDA, for Au$_{140}$(C6)$_{53}$ chemically charged to −191 mV vs Ag/Ag$^+$. Inset: Cartoon of electron conduction in a mixed-valent MPC film.

swept over ±1 V at 100 mV/s; results were unchanged at 5, 10, and 200 mV/s, with no evidence of hysteresis. At least two measurements, and usually three, were taken for each σ_{EL} data point; standard deviations were generally <2%. Some films were measured using ac impedance spectroscopy from 1 MHz to 1 Hz, which agreed within ±5%. Complex plane diagrams typically showed a semicircle from which a resistance could be determined.

The conductivities reported are obviously not the maximum achievable values in MPC films since $\Delta i/\Delta E$ increases at higher voltage biases. Some properties of conductivity at larger voltage biases were discussed in the earlier paper.[8]

MPC Concentration. The concentration of MPC cores within a film determines their average center-to-center and edge-to-edge separations. The concentration of Au$_{140}$(C6)$_{53}$ MPCs in a solid sample is 0.10 ± 0.03 M as evaluated from a pychnometrically[22a] measured density (pycnometry is a volume displacement measurement). Core concentrations were similarly evaluated for the series of Au$_{309}$(C$_n$)$_{92}$ MPCs; their core edge-to-edge distances[22a] were calculated from MPC radii assuming a hexagonal close packed (hcp) model (fill factor 0.73) and the 1.1 nm average core radius. Comparing experimental core edge-to-edge distances to the lengths of extended alkanethiolate chains shows that the latter exceeds the former by factors of 1.0 to 1.4, with an average of 1.2 ± 0.2 and no obvious trends. This finding reflects the interdigitation of the monolayer chains (or bundles thereof[2i]) that has been established, by computation[2i] and TEM observations,[15a] to occur for alkanethiolate MPCs. In TEM, for example, the edges of the Au cores can be seen[15a] to be spaced by distances slightly more than the length of a single alkanethiolate chain. In solid-state MPC films, the average edge-to-edge core separation is 1.2-fold larger than the length of a *single* chain due to this interdigitation. Thus, in the context of MPC core edge-to-edge distance, the usual[6a] 1.25 Å/CH$_2$ for an alkanethiolate monolayer corresponds to 1.5 Å/CH$_2$.

Results and Discussion

Chemical Charging of MPC Cores. Electronic charging of alkanethiolate MPC cores can be accomplished[21] by electrolysis and the charged materials can be dried as stable solids. Chemical

(18) Measurements in refs 6a and 6b were vs AgCl quasireference electrodes (QRE), whereas those in this paper used a Ag/Ag$^+$ (0.01M AgNO$_3$ in CH$_3$CN) reference electrode whose potential was roughly −50 mV vs the QRE, by mutual reference to the oxidation wave of tetracyano-quinodimethane.

(19) (a) Wooster, T. T.; Longmire, M. L.; Zhang, H.; Watanabe, M.; Murray, R. W. *Anal. Chem.* **1992**, *64*, 1132. (b) Chidsey, C. E. D.; Feldman, B. J.; Lundgren, C.; Murray, R. W. *J. Am. Chem. Soc.* **1986**, *58*, 601.

(20) We assume that tetrabutylammonium (TBA) or perchlorate serve as counterions to the negatively or positively charged MPCs.
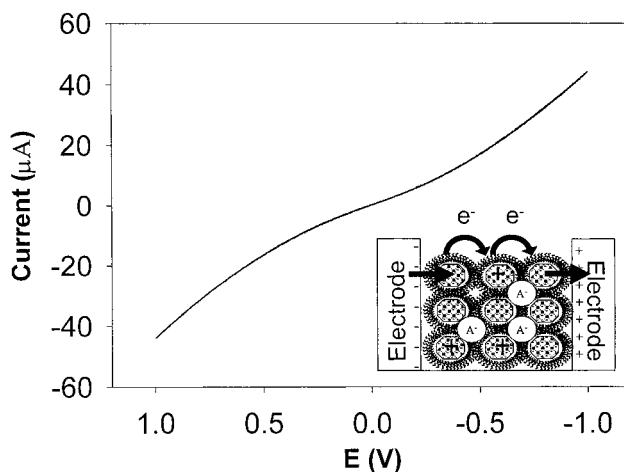
(21) Pietron, J. J.; Hicks, J. F.; Murray, R. W. *J. Am. Chem. Soc.* **1999**, *121*, 5565.

(22) (a) Pietron, J. J.; Murray, R. W. Unpublished data, University of North Carolina. MPC films were drop-cast into a 2 mL pychnometer with water used as the displacement liquid. (b) For example, densities, concentrations, and edge-to-edge distances for R = C8, C12, and C16 were 3.32 ± 0.24, 3.06 ± 0.07, 2.70 ± 0.15 g/cm^3, 0.033, 0.029, 0.022 M, and 1.31 ± 0.08, 1.48 ± 0.03, 1.83 ± 0.07 nm respectively. Alkanethiolate ligand chain lengths (calculated by HyperChem software) are C16 = 2.02 nm, C12 = 1.52 nm, C10 = 1.27 nm, C9 = 1.02 nm, C7 = 0.90 nm, C6 = 0.77 nm, C5 = 0.65 nm, and C4 = 0.52 nm.

11468   *J. Am. Chem. Soc., Vol. 122, No. 46, 2000*

Wuelfing et al.

Table 1. Chemical Charging of $Au_{140}(C6)_{53}$ MPCs

rest potential (mV vs Ag/Ag$^+$)[a]	no. of exposures to Ce(SO$_4$)$_2$ soln (5 mM)	stir time (min)	post-conductivity rest potential (mV vs Ag/Ag$^+$)[b]
−611	none/as-prepared	0	−611
−411	1[c]	0.5	−414, −401[d]
−300	1[c]	0.5	
−296	1	1	
−240	1	1.5	
−221	1	2.5	
−212	1	2	
−191	1	5	−180
−163	1	5	−156
−90	1	12	−84
−35	1	11	-
26	1	12	35
115	2[e] (−100 mV)	10,10[e]	-
223	4[e] (−133, −20, 97 mV)	17,10,10,10[e]	-

[a] Rest potential of solution charged using Ce(IV). [b] Solution potential measurements made after redissolving MPC films from IDAs. [c] That the same charging time produced two different rest potentials simply reflects the difficulty of reproducing contact times and areas in a stirred heterogeneous mixture over a short time scale. [d] Measurement without added supporting electrolyte. [e] Multiple charging steps were needed to achieve the listed sample potential; intermediate rest potentials given in parentheses. The intermediate potentials, before re-exposure to Ce(SO$_4$)$_2$, are in parentheses.

charging was studied in this paper, aiming at a procedure that can provide larger quantities of charged materials for the present and other purposes such as study of optical[9] and solubility[21] properties.

CH$_2$Cl$_2$ solutions of $Au_{140}(C6)_{53}$ MPCs were charged by emulsifying with an aqueous oxidant solution (Ce(SO$_4$)$_2$). The rest potentials (Table 1) of the resulting mixed-valent CH$_2$Cl$_2$ solutions became more positive (more positive average MPC core charge) with increasing contact time with the oxidant solution. Multiple exposures to fresh Ce(SO$_4$)$_2$ solution were required to charge the MPCs more positively than ca. 100mV vs Ag/Ag$^+$. A 50-fold molar excess of Ce(SO$_4$)$_2$ (relative to MPC) was employed, meaning that the charging process is both slow and much less than quantitative. The most positively charged MPC solutions obtained correspond to removal of two electrons from each MPC core, which is less positively charged than was achieved in the electrolytic procedure.[21]

Rest potentials of solutions of as-prepared $Au_{140}(C6)_{53}$ MPCs were sometimes more negative than the potential of zero charge (PZC) of the MPCs,[6a,b] indicating that the reduction step in their synthesis leaves a residue of reductive charge on the MPC. This effect was not very reproducible, residual charge is not always observed, and in this study, the initial rest potentials varied between −350 and −611 mV. The latter potential corresponds to a solution of MPC^{1-} containing a small amount of MPC^{2-} (see below).

MPC Charge State Determination. $Au_{140}(C6)_{53}$ MPCs dissolved in an electrolyte solution exhibit[4a,6a,b,c] well-defined voltammetric current peaks that correspond to serial, one-electron charging of the MPCs' electrical double layers ("quantized double layer charging", QDL). Figure 2(lower, —) shows an illustrative differential pulse voltammogram. The PZC is indicated on the figure; at this potential, MPCs at the electron/solution interface have uncharged cores. That a single electron can change the potential of an MPC by ca. 300 mV is due to the tiny (ca. 0.5 aF) double layer capacitance per MPC, which as we have discussed,[4a,6,a−c] is due to the small MPC core dimension and monolayer dielectric constant.

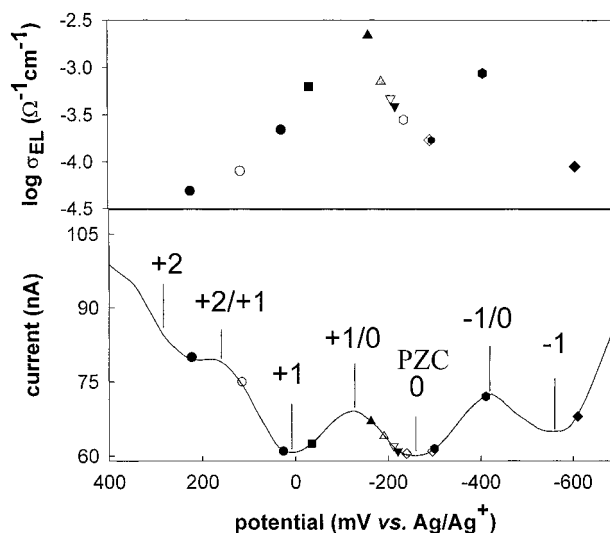Each one-electron MPC charging step can be *formally* regarded as a "redox" transformation, and assigned (vs E_{PZC}) a

Figure 2. (Top) 30 °C electronic conductivity vs rest potential (mV vs Ag/Ag$^+$) of the solution from which the solid-state, mixed-valent MPC film was cast. The rest potentials are listed in Table 2. (Bottom) Differential pulse voltammogram (DPV) of 96 μM $Au_{140}(C6)_{53}$/0.1 M Bu$_4$N$^+$ClO$_4^−$ in CH$_2$Cl$_2$ at a 0.6 mm Pt working electrode (nonaqueous Ag/Ag$^+$ (0.01 M AgNO$_3$) reference and Pt coil counter electrodes). The points on the DPV trace are the solution rest potentials.

pseudo-formal potential $E^{o\prime}$. At the potential of the current peak, equal concentrations of a charge state "couple" (e.g., MPC^0 and MPC^{1+}) exist at the electrolyte/solution interface. At potentials off the peak, relative concentrations of the charge state "couple" can be calculated using the Nernst equation,[23]

$$E - E^{o\prime} = 0.059 \log \frac{[MPC^{z+1}]}{[MPC^z]} \quad (4)$$

Rest potentials of chemically charged MPC solutions represent bulk as well as interfacial solution concentrations. The voltammetry of Figure 2 (lower, —) provides the $E^{o\prime}$ landmarks for the calculation—using eq 4—of the [MPC^{z+1}]/[MPC^z] ratios in the solutions. The rest potentials measured are indicated by points on the Figure 2 (lower) DPV trace. A rest potential of −191 mV corresponds, for example, to a solution of predominantly MPC^0 with a minority of MPC^{1+}. While 13 different mixed-valent solutions were prepared, by chance none happened to result in an exact 1:1 ratio of any of the charge state couples.

The solid-state films cast from the solutions with the above rest potentials have the same relative proportions of [MPC^{z+1}] and [MPC^z] sites that were in the solution. That is, the films have a known mixed valency, or level of doping. Actual solid-state concentrations are obtained using pycnometrically determined solid-state $Au_{140}(C6)_{53}$ concentration (0.01 M). Upon redissolving the films in CH$_2$Cl$_2$ after conductivity measurements, the resulting solution potential generally was within ±10 mV of the original value, with or without adding supporting electrolyte. *MPC solution rest potentials and the potentials of solid-state films can be considered as equivalent in regards to the mixed-valent composition of the film.*

Conductivity of Mixed-Valent MPCs. We have posited that reaction 1 can be used to represent the electronic conductivity of mixed-valent solid-state MPCs. Figure 2(upper) and Table 2 present conductivities measured at 30 °C as a function of the rest potentials of the 13 different mixed-valent $Au_{140}(C6)_{53}$ MPC samples. Consider first the ca. 0 to −250 mV potential interval,

(23) Bard, A. J.; Faulkner, L. *Electrochemical Techniques: Fundamentals and Applications*; Wiley and Sons: New York, 1980.

Table 2.   Electronic Conductivities and Self-Exchange Rate Constants for $Au_{140}(C6)_{53}$ MPCs

charge couple[a]	$Au_{140}(C6)_{53}$ film potential (mV vs. Ag/Ag$^+$)[b]	σ_{EL} (30 °C)[c] (Ω^{-1} cm^{-1})	film composition charge state (%)[d]					bimolecular rate constant k_{EX} (M^{-1}s^{-1})[e]
			+2	+1	0	−1	−2	
MPC$^{2+/1+}$	223	4.9×10^{-5}	87.1	12.9				7×10^8
	115	8.0×10^{-5}	9.1	90.9				2×10^9
	26	2.2×10^{-4}	3.1	96.9				1×10^{11}
MPC$^{1+/0}$	−35	6.3×10^{-4}		97.2	2.8			4×10^{10}
	−163	2.2×10^{-3}		19.1	80.9			2×10^{10}
	−191	7.1×10^{-4}		7.3	92.7			2×10^{10}
	−212	4.7×10^{-4}		3.4	96.6			3×10^{10}
	−221	3.9×10^{-4}		2.4	97.6			4×10^{10}
	−240	2.8×10^{-4}		1.2	98.8			4×10^{10}
MPC$^{0/1-}$	−296	1.7×10^{-4}			99.3	0.7		4×10^{10}
	−300	1.7×10^{-4}			99.2	0.8		4×10^{10}
	−411	8.7×10^{-4}			62.4	37.6		6×10^9
MPC$^{1-/2-}$	−610	8.9×10^{-5}				99.4	0.6	2×10^{10}

[a] Determined by inspection of DPV in Figure 2. [b] Determined by solution rest potential measurement. [c] From slope of I−V curves of MPC films. [d] Determined by Nernst equation and DPV-determined $E^{o\prime}$. $E^{o\prime}(MPC^{1-/0}) = -424$ mV, $E^{o\prime}(MPC^{1+/0}) = -126$ mV, $E^{o\prime}(MPC^{2+/1+}) = 174$ mV. [e] Calculated by eq 5.
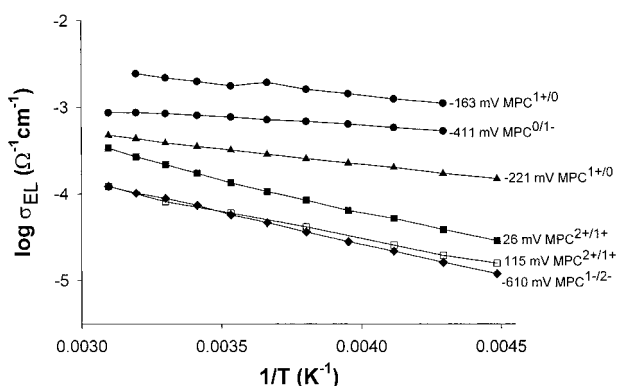
Figure 3. Arrhenius plot of selected solid-state, mixed-valent MPC films. MPC film potential and charge composition are listed beside each line.

which encompasses films with MPC$^{0/1+}$ mixed valencies. It is evident in Figure 2 (upper) that the conductivity within this set of seven films smoothly moves to higher values as the concentration ratio [MPC^{1+}]/[MPC^0] approaches unity. The conductivity variations are ca. 10-fold. For a bimolecular reaction, the rate should maximize at [MPC^{1+}]/[MPC^0] = 1.

The results are analyzed by a hypothetical cubic lattice model previously applied[10b] to electron transport in redox polymers,

$$k_{EX} = \frac{6RT\sigma_{EL}}{10^{-3}F^2\delta^2[MPC^0][MPC^{1+}]} \quad (5)$$

where k_{EX} is the electron self-exchange rate constant (M^{-1} s^{-1}), R the gas constant, σ_{EL} the conductivity (Ω^{-1} cm^{-1}) at temperature T (K), F the Faraday constant, and δ the core center-to-center distance (cm). Table 2 gives results for MPC$^{0/1+}$ k_{EX} values, from which two observations can be made. First, while the conductivity within the MPC$^{0/1+}$ series varies by ca. 10-fold, k_{EX} is relatively constant, consistent with the bimolecular model. Second, the obtained rate constant is very large, exceeding 10^{10} M^{-1} s^{-1}. The corresponding first order rate constant is ca. 10^8 s^{-1}. We know of no precedent literature for comparison to this large value.

Arrhenius plots for the conductivities of selected charge state couples shown in Figure 3 give the thermal activation barrier energies in Table 3. The electron self-exchange barriers for the MPC$^{0/1+}$ couple are roughly independent of charge state—6.7 ± 0.7 kJ/mol or 0.069 ± 0.01 eV (excluding the −35mV data point)—and are small in comparison to the 0.21 eV barrier

Table 3.   Activation Energies for Mixed-Valent $Au_{140}(C6)_{53}$ MPC Films

charge couple[a]	$Au_{140}(C6)_{53}$ film potential (mV vs Ag/Ag$^+$)[b]	E_A, Arrhenius plots (kJ/mol)[c]	$E_{A,GM}$ ln σ_{el} vs $T^{-1/2}$ (kJ/mol)[d]
MPC$^{2+/1+}$	223	10.6	2.1
	115	12.2	2.9
	26	14.6	4.2
MPC$^{1+/0}$	−35	14.8	4.3
	−163	5.6	0.6
	−191	7.4	1.1
	−212	6.0	0.7
	−221	6.8	0.9
	−240	7.7	1.2
MPC$^{0/1-}$	−296	4.5	0.4
	~E_{PZC}	(calcd 6.7)[e]	(calcd 15.6)[f]
	−300	4.1	0.3
	−411	3.5	0.2
MPC$^{1-/2-}$	−610	14.0	3.8

[a] Determined by inspection of DPV in Figure 2. [b] Determined by solution rest potential measurement. [c] Activation energy from Arrhenius plots (ln σ_{EL} vs 1/T). [d] Activation energy from granular metal plots of (ln σ_{el} vs 1/$\sqrt{T}$). [e] Calculated by eq 8. Chain lengths used for alkanethiolate ligands were calculated by HyperChem software. C16 = 2.02 nm, C12 = 1.52 nm, C10 = 1.27 nm, C9 = 1.02 nm, C7 = 0.90 nm, C6 = 0.77 nm, C5 = 0.65 nm, and C4 = 0.52 nm. Chain interdigitation was taken into account for all calculations. [f] Calculated by eq 9.

observed[14a] for ferrocene attached to a Au electrode by hexanethiolate chains. The small barrier energy is certainly one source of the large MPC$^{0/1+}$ k_{EX} rate constants. Uncertainties in the k_{EX} results include the simplistic cubic lattice model underlying eq 5 and approximating the IDA as a parallel plate conductivity cell; however, the same approximations were made in studies of mixed-valent redox polymers,[10] where much smaller rate constants were encountered.

For the other MPC mixed-valent couples, there are fewer results (Table 2) and the behavior is less clear. The data do seem to be fairly reproducible (note the results at rest potentials of −296 and −300). At more negative potentials, i.e., the MPC$^{0/1-}$ charge state couple, conductivity increases when the concentration ratio [MPC^{1-}]/[MPC^0] approaches unity, but k_{EX} is not as consistently constant as for the MPC$^{0/1+}$ charge state couple. At more positive potentials, the k_{EX} decreases. Table 3 and Figure 2 show that barrier energies for the highly charged couples, MPC$^{1+/2+}$ and MPC$^{1-/2-}$, become decidedly larger. The most highly charged films contain larger counterion populations and also, possibly, other counterions than perchlorate owing to

details of the preparation; perhaps the resulting Coulombic interactions contribute to increased barrier energies. The regimes of highly charged mixed-valent MPC conductivity await a more detailed inspection than provided here.

It is useful to consider the conductivity of a neutral, non-"mixed-valent" MPC, in comparison to that of a mixed-valent one. The film with a −296 mV rest potential (99.7% MPC^0, Table 2), which is very close to overall neutral, exhibits a conductivity that, while smaller than those of the mixed-valent films, is still quite appreciable. The conductivity of this film would depend on a charge carrier population thermally generated by the disproportionation reaction.

$$2MPC^0 \rightarrow MPC^{1+} + MPC^{1-} \qquad (6)$$

This reaction induces a small degree of mixed-valent conductivity. The room-temperature equilibrium constant of reaction 6 is 1.1×10^{-5}, which is obtained using the ~300 mV separation (Figure 2, lower) between $E^{o\prime}$ for the MPC$^{0/1+}$ and MPC$^{0/1-}$ charge state couples.[24] Given this constant, ca. 0.7% of the cores in an overall neutral Au$_{140}$(C6)$_{53}$ MPC^0 film at thermal equilibrium would be charged as either MPC^{1+} or MPC^{1-}, which according to eq 5 should produce a conductivity ca. 22-fold and 34-fold less than that of films that are 1:4 [MPC$^+$]/[MPC^0] (−163mV sample) and 1:1.5 [MPC^{1-}]/[MP^0] (−411 mV sample), respectively. The actual differences (Table 2), factors of 13-fold and 5.1-fold, respectively, are somewhat less than the estimate, so the overall neutral film is somewhat more conductive than expected. The reason for the higher MPC$^{0/1+}$ couple conductivity is unknown at this point.

It is important to recognize that charge carrier generation by disproportionation, i.e., reaction 6, will be more efficient for MPCs with larger core sizes or higher dielectric constant monolayers than the Au$_{140}$(C6)$_{53}$ MPC, since those properties lead[6a] to larger MPC capacitance and smaller spacing between $E^{o\prime}$ values. The capacitance of the Au$_{140}$(C6)$_{53}$ MPC is 0.5 aF.[6a] Were the MPC double layer capacitance as large as ca. 6.4 aF, the $E^{o\prime}$ spacing would fall to less than k_BT_{298} (which is 25 mV), where k_B is the Boltzmann constant. An MPC with a C6 alkanethiolate monolayer (dielectric constant = 3) and a 3.5 nm core diameter would have[6a] such a capacitance. Thus, for MPCs or other nanoparticles of this and larger capacitance, mixed valency conductivity enhancement will not be readily observable, since nearly as many, or more, carriers will be generated by the disproportionation reaction 6. Observable mixed-valent conductivity is a province of MPCs, and other nanoparticles, for which discretized charging like the voltammetry of Figure 2 (lower, −) can be seen.

As a final observation on thermal charge carrier generation in solid-state, nonmixed-valent MPCs, we earlier[8] employed the conductivity activation barrier energy in a Boltzmann expression to estimate an equilibrium carrier (i.e., MPC^{1+} and MPC^{1-}) concentration. The conductivity activation barrier energy refers, however, to reaction 1 (electron transport), not reaction 6 (generation), and is smaller, and using this energy in the Boltzmann expression overestimated the thermal MPC$^{1+/1-}$ carrier population.

Chain Length Dependence on Conductivity. Seeking further information on chain length effects[2j,8] on electronic conductivity, especially for shorter chains, measurements were conducted on C4, C5, C6, C7, and C10 versions of Au$_{309}$(C$_n$)$_{92}$ MPCs, to add to the previous[8] C8, C12, and C16 results. The

(24) K was calculated from $nF(E − E^{0\prime}) = RT \ln K$ where $K = $ [MPC^{1+}]-[MPC^{1-}]/[MPC^0].
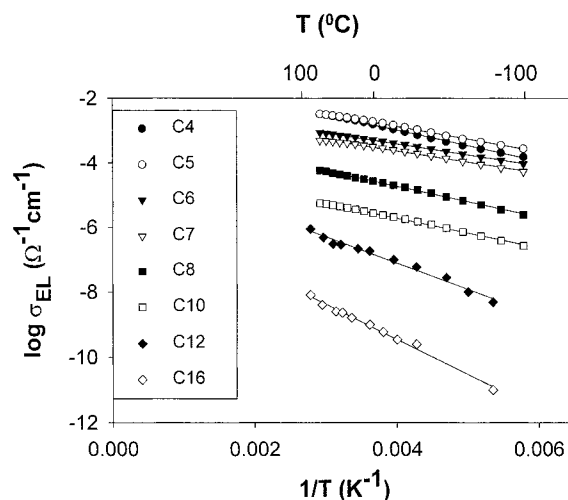

Figure 4. Arrhenius plot of electronic conductivities of a series of Au$_{309}$(C$_n$)$_{92}$ MPCs with varying alkanethiolate chain lengths.

relevant relation[8] is

$$\sigma_{EL}(n,T) = \sigma_o \exp[-n\beta_n] \exp[-E_A/RT] \qquad (7)$$

where n is alkanethiolate chain length, β_n the corresponding electronic coupling term, and E_A the activation energy of conductivity (kJ/mol). The preexponential term $\sigma_o e^{-n\beta}$ (Ω^{-1} cm^{-1}) is the equivalent of an infinite-temperature electronic conductivity.

The conductivity results are shown in Figure 4 as Arrhenius plots; activation barrier energies and intercepts ($\sigma_o e^{-n\beta}$) are given in Table 4. The effect of chain length on conductivity is large, as expected for an electron tunneling transport mechanism. The conductivity changes parallel those in chain lengths except for the inversion of the C4 and C5 chain length conductivities seen at lower temperatures. Figure 5 shows plots of the chain length dependence according to eq 7; the slopes give $\beta_n = 1.2$ (70 °C), 1.2 (30 °C), and 1.5 (−60 °C) per carbon unit. The apparent temperature dependence of β_n arises through the larger activation barrier energies at the longer chain lengths (see Table 4). The variation in E_A can in principle[8] be avoided by plotting the Arrhenius intercepts $\ln(\sigma_o e^{-n\beta})$ against n. The intercepts of course have uncertainties associated with the long extrapolation. This plot (Figure S-2) is linear and yields $\beta_n = 0.9$ Å^{-1}.

To express the electronic coupling term in the conventional Å^{-1} units (β_{dis}) requires translating n into MPC core edge-to-edge distance. $\beta_{dis} = \beta_n/1.5$, as discussed in the Experimental Section. The conversion factor is larger than the usual[6a] length per methylene (1.25 Å/carbon unit) because of alkanethiolate chain intercalation giving an average core edge-to-edge distance equal to 1.2-fold the length of an extended MPC monolayer chain (see schematic inset in Figure 5).[21] The resulting values at the three temperatures are $\beta_{dis} = 0.8, 0.8,$ and 1.0 Å^{-1}, respectively, and 0.6 for the intercept plot. These results lie within the range of values computed for electron donor−acceptor pairs connected by trans-staggered alkane chains.[26] They are somewhat smaller (and also less refined) than the ~1 Å^{-1} result of experiments on ferrocene alkanethiolate monolayers on Au electrodes.[14]

Figure 5 contains two features that, while somewhat indistinct, are repeated at each of the three temperatures. At the shortest,

(25) $C_{CLU} = 4\pi\epsilon\epsilon_0(r/d)(r + d)$, where r is the radius of the MPC and d is the monolayer length.[6a]

(26) Curtiss, L. A.; Naleway, C. A.; Miller, J. R. *J. Phys. Chem.* **1993**, *97*, 4050.

Table 4.　Activation Energies of $Au_{309}(C_n)_{92}$ MPCs MPCs

$Au_{309}(C_n)_{92}$ alkanethiolate (carbon units)	E_A, Arrhenius plots (kJ/mol)[a]	Arrhenius Plot intercepts $\log[\sigma_{EL}(e^{-n\beta})(\Omega^{-1}\,cm^{-1})]$[b]	calcd E_A, Marcus theory (kJ/mol)[c]	$E_{A,GM}$ ln σ_{el} vs $T^{-1/2}$ (kJ/mol)[d]	calcd $E_{A,GM}$ granular model (kJ/mol)[e]
C16	19.0	-5.9 ± 0.3	5.4	4.9	14.6
C12	16.0	-4.1 ± 0.3	5.2	3.6	13.2
C10	8.8	$-3.9 \pm <0.1$	5.0	1.5	12.3
C8	9.1	$-2.8 \pm <0.1$	4.8	2.0	11.1
C7	6.6	$-2.3 \pm <0.1$	4.7	1.2	10.4
C6	6.5	$-2.1 \pm <0.1$	4.6	1.3	9.6
C5	7.5	$-1.3 \pm <0.1$	4.5	2.0	8.8
C4	9.2	$-1.1 \pm <0.1$	4.4	3.9	7.7

[a] Activation energy from Figure 4 Arrhenius plots (ln σ_{EL} vs $1/T$). [b] Intercepts of Arrhenius plots, with uncertainties, from Figure 4. [c] Calculated by eq 8. Chain lengths used for alkanethiolate ligands were calculated by HyperChem software. C16 = 2.02 nm, C12 = 1.52 nm, C10 = 1.27 nm, C9 = 1.02 nm, C7 = 0.90 nm, C6 = 0.77 nm, C5 = 0.65 nm, and C4 = 0.52 nm. Chain interdigitation was taken into account for all calculations. [d] Activation energy from granular metal plots (ln σ_{el} vs $1/\sqrt{T}$). [e] Calculated by eq 9.
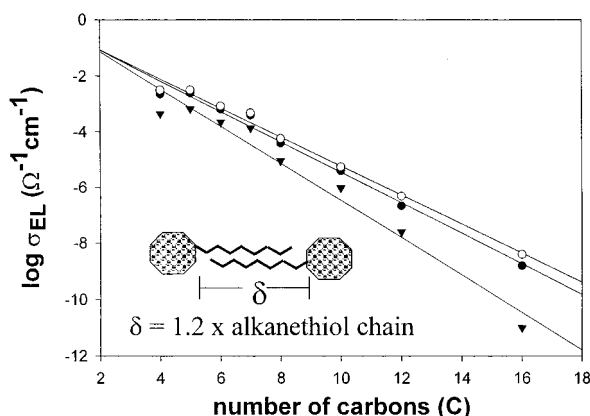

Figure 5. Plot of 70 (○), 30 (●), and −60 °C (▼) conductivity vs number of carbons in the alkanethiolate chains of $Au_{309}(C_n)_{92}$ MPCs (eq 7). The inset is a schematic describing the interdigitation of monolayer chains in solid-state MPC films.

C4 and C5, chain lengths, the plot folds over. A slight fold-over in the electronic coupling between electron donor−acceptor groups bridged by methylene chains has been predicted[27] for the C2,C3 interval, and was observed to occur in the C6,C7 interval in a ferrocene alkanethiolate monolayer study.[14a] A plot of $\log[\sigma_{EL}(e^{-n\beta})]$ against n (Figure S-2) does not, however, show a fold-over. The second interesting, but quite faint, feature of Figure 5 is the C4 to C7 interval, which exhibits an odd−even irregularity.

The exponential relationship of Figure 5 confirms that conductivity is dominated by electronic tunneling through the alkanethiolate matrix between MPC cores. This study was designed to probe the conductivity mechanism rather than to maximize conductivity. A wide range of conductivity (ca. 10⁶-fold) is obtained by choice of alkanethiolate monolayer chain length; the ability to design conductivity characteristics can be useful in designing nanoscale electronic devices.[6d] Results from self-assembled monolayers containing conjugated ligands[29] ($\beta \sim 0.5$ Å^{-1}) suggest that conductivities of MPC with conjugated monolayers will be significantly increased.

$Au_{309}(C_n)_{92}$ MPC conductivities could not be translated into self-exchange rate constants, primarily because this MPC preparation[2p,8,15a] has a large dispersity in core size. Poly-disperse MPCs give featureless current−potential double layer charging responses, i.e., not discrete peaks seen in Figure 2

(27) Lui, L. L.; Newton, M. D. *J. Phys. Chem.* **1994**, *98*, 7162.
(28) Hyat, W. H. *Engineering Electromagnetics*; McGraw-Hill: New York, 1989.
(29) Hsung, R. P.; Chidsey, C. E. D.; Sita, L. R. *Organometallics* **1995**, *14*, 4808.

(lower). Additionally, even if the $Au_{309}(C_n)_{92}$ MPC sample were monodisperse, its larger core size would depress the $E^{o\prime}$ spacing below that in Figure 2 (lower), to ca. 60 mV.[6a] Finally, rest potentials were not measured (at the time of these conductivity measurements the potential significance of core charge was not recognized), and there is some uncertainty as to whether all of the $Au_{309}(C_n)_{92}$ MPC preparations were in a neutral state. (A solution made from a more recently synthesized sample of Au_{309}-$(C_n)_{92}$ MPCs did not exhibit the negative rest potentials typical of $Au_{140}(C6)_{50}$ MPCs, so larger core MPCs may not retain residual charge as effectively as small ones.)

We know very little about the effect of MPC core size on conductivity. Some preliminary data have been collected. Room-temperature conductivities for as-prepared C4, C6, and C12 $Au_{140}(C_n)_{53}$ MPC films (multiple measurements on individual drop-cast films − standard deviation < 5%) were 5.9×10^{-3}, 1.8×10^{-4}, and 2.1×10^{-7} Ω^{-1} cm^{-1}, respectively; corresponding values for $Au_{309}(C_n)_{92}$ MPCs are 2.3×10^{-3}, 6.6×10^{-4}, and 3.0×10^{-7} Ω^{-1} cm^{-1}, respectively. These values are not very different, suggesting that small changes in core size (1.6 nm vs 2.2 nm diameters) have relatively minor effects on MPC conductivity.

Activation Energies. This section will focus on comparing the activation barrier energy results for $Au_{309}(C_n)_{92}$ MPCs with varied monolayer chain lengths (Table 4) to the theories for electron transfers known as Marcus[13] theory and granular metal or Cermet[12] theory. The question is whether these theories predict barrier energies and chain length dependencies similar to the experimental findings.

Marcus theory, based[13] on the energetics of repolarization in a dielectric continuum medium, gives the free energy of activation ΔG^* expression

$$\Delta G^* = \frac{\lambda}{4} = \frac{e^2}{16\pi\epsilon_0}\left(\frac{1}{2r_1} + \frac{1}{2r_2} - \frac{1}{r}\right)\left(\frac{1}{\epsilon_{op}} - \frac{1}{\epsilon_s}\right) \qquad (8)$$

where λ is the "outer-sphere" reorganizational energy, r_1 and r_2 are radii of neighboring MPCs (ideally equal), r is the center-to-center MPC distance (m), and ϵ_{op} and ϵ_s are the medium optical and static dielectric constants, respectively. For a symmetrical electron self-exchange reaction, the entropic energy of activation is zero[13] so that ΔG^* equals the enthalpic (experimental) energy barrier E_A. Equation 8 contains a dependency on MPC monolayer chain length in the distance terms and on the monolayer chemistry in the dielectric parameters. The average $Au_{309}(C_n)_{92}$ MPC core radius (r_1 and r_2) is 1.1×10^{-9} m; the center-to-center distance varies with alkanethiolate chain length. (It must be remembered that the $Au_{309}(C_n)_{92}$ MPCs are polydisperse so that an assortment of

distances is actually present.) The optical dielectric constant ϵ_{op} is assumed to be that of pentane $\epsilon_{op} = 1.3$,[31] and the static one, $\epsilon_S = 3$, was determined by studies of alkanethiolate SAMs on Au electrodes[30] and was successfully used to account for double-layer charging of MPCs in solutions.[6a] (Using $\epsilon_S = 3$ ignores the possible contributions of neighbor MPC core electronic repolarization to the dielectric environment of an MPC electron-transfer reactant.) Marcus ΔG^* values calculated given these assumptions and parameters are shown in Table 4.

The experimental Arrhenius E_A values for the $Au_{309}(C_n)_{92}$ MPC series (Table 4) fall roughly into two groups: shorter chain length (C4 to C10) MPCs with relatively constant barrier energies (8.0 ± 1.1 kJ/mol or 0.083 ± 0.01 eV) and C12 and C16 MPCs with much larger barrier energies. Over the C4 to C10 MPC range, the Marcus eq 8-calculated ΔG^* barrier energies decrease by about 10% (5.0 to 4.5 kJ/mol). Unfortunately, this change is comparable to the experimental uncertainty of Arrhenius E_A for this series of MPCs. While the average experimental E_A is somewhat larger than the average calculated ΔG^*, the ca. 1.7-fold difference is larger than the experimental uncertainty, but potentially not the uncertainties (noted above) of the parameters used in the theoretical calculations. For the $Au_{140}(C6)_{53}$ MPC (Table 3), eq 8 predicts a barrier energy of 6.7 kJ/mol, a value ca. 1.5-fold larger than the 4.5 kJ/mol measured for the approximately charge-neutral −296 mV Au_{140}-$(C6)_{53}$ sample. At least for MPCs with shorter chain lengths, the experimental activation behavior is not inconsistent with Marcus theory predictions, but does not allow fine distinctions to be drawn.

The E_A results for C12 and C16 MPCs are, on the other hand, more clearly discordant with eq 8. Monolayers of C12 and C16 MPCs exhibit[15a] some crystallinity at room temperature, whereas shorter chain length MPCs do not, which might explain the differences. The Arrhenius plots (Figure 4) for the C12 or C16 MPCs do not, however, display any peculiarities at their melting temperatures. Also, the C12 and C16 MPC density measurements showed that their alkanethiolate chains interdigitate to the same extent as the shorter chain MPC films, suggesting that factors other—and as yet unknown—than solid-state ordering or packing cause the barrier increase.

The granular metal conductivity model has been studied extensively[12] for systems such as 2−20000 Å metal (Au, Ag, Ni) grains dispersed below the percolation threshold in a dielectric medium, such as SiO_2 particles of the same order of size. The theory can be categorized into so-called low-field and high-field conductivity regimes.[12] The MPCs fall into the smaller dimension range of this literature, and our experiments into the low-field regime. In this regime, the applied bias produces voltage drops between neighboring particles that are smaller than thermal energy, $k_b T_{298} \approx 25$ mV, so that charge carrier generation occurs by eq 6. For the $Au_{309}(C_n)_{92}$ MPCs, a ±1 V bias corresponds to <1 mV between MPCs, and the energy requirement of eq 6 is ≈60 mV.

In the low-field regime, $\sigma_{EL} = \sigma_0 \exp[-2(C_0/RT)^{1/2}]$, where $C_0 = 2\beta\delta E_{A,GM}(1 + (^1/_2\beta\delta))$, and the activation barrier energy $E_{A,GM}$ is given by

$$E_{A,GM} = \frac{\frac{1}{2}e^2\left[\frac{1}{r} - \frac{1}{r+\delta}\right]}{4\pi\epsilon_0\epsilon} \qquad (9)$$

where r is the particle radius and ϵ is the dielectric constant of the intervening medium.[2b,12a] The other parameters are as described above. Plotting the conductivity results from the linear current−voltage region (Figure 1) for $Au_{309}(C_n)_{92}$ MPCs as ln-$[\sigma_{EL}]$ vs $1/\sqrt{T}$, and using $\beta = 0.8$ Å^{-1}, produces the granular metal activation barrier energies ($E_{A,GM}$) in Table 4. Table 4 also gives barrier predictions calculated from eq 9. These are larger than those from Marcus theory and considerably larger (by 3- to 10-fold) than those ($E_{A,GM}$) from the experimental ln-$[\sigma_{EL}]$ vs $1/\sqrt{T}$ plots. The predicted granular metal barrier energy (15.6 kJ/mol) for the $Au_{140}(C6)_{53}$ MPCs for the nonmixed-valent (−296 mV) sample (Table 3) is also much larger than the experimental $\ln[\sigma_{EL}]$ vs $1/\sqrt{T}$ plot values.

We conclude that Marcus formulation provides a somewhat more consistent—albeit still imperfect—representation of the activation barrier energies in these materials than does the granular metal model, which predicts barrier energies larger than are observed. At this point, it is also clear that the comparison with theory leaves many questions for future studies.

Note Added in Proof: (a) The ca. 10^8 s^{-1} rate constant for the MPC$^{0/1+}$ corresponds to (RTN_A/F^2k) a molecular resistance element of ca. 10^9 Ω for the bundle of hexanethiolate chains interposed between adjacent Au cores. (b) Reed, M. A.; Zhou, C.; Muller, C. J.; Burgin, T. P.; Tour, J. M. *Science* **1997**, *278*, 252−254.

Supporting Information Available: Schematic of interdigitated electrodes used to collect conductivity data and plot of $\log[\sigma_{EL}(e^{-n\beta})]$ intercepts of Arrhenius plots against n (PDF). This material is available free of charge via the Internet at http://pubs.acs.org.

(30) Chidsey, C. E. D.; Loiciano, D. N. *Langmuir* **1990**, *6*, 682.
(31) Lide, D. R., Ed. *CRC Handbook of Chemistry and Physics*, 72nd ed.; CRC Press: Boca Raton, FL, 1992.